Alexandria Engineering Journal (2022) 61, 701–708

HOSTED BY

Alexandria University

Alexandria Engineering Journal

www.elsevier.com/locate/aej
www.sciencedirect.com

Visibility enhancement of underwater images based on active polarized illumination and average filtering technology

Tianci Li [a,b], Jianli Wang [a], Kainan Yao [a,*]

[a] Changchun Institute of Optics, Fine Mechanics and Physics, Chinese Academy of Sciences, Changchun 130033, China
[b] University of Chinese Academy of Sciences, Beijing 100049, China

Received 25 February 2021; revised 21 April 2021; accepted 13 June 2021
Available online 23 June 2021

KEYWORDS

Polarized illumination;
Dehazing;
Average filtering

Abstract Underwater imaging is a crucial and challenging problem. The backscattering caused by particles in turbid water can severely degrade the image. In this paper, A novel image dehazing method is devised, which combines optics with image processing technology. This method can directly remove part of the backscattering through polarization technology, and then quickly solve the dehazing image through our algorithm. Experimental results show that our method is valid and robust for targets of diverse materials, grayscale images and color images in diverse scattering environments. Furthermore, our method takes only 2 percent of the time of the fast dark channel prior (DCP) method when processing 1 K resolution images, which meets the requirements of real-time.

1. Introduction

Underwater imaging has a crucial application value in the area of seabed mineral resource exploration, submarine pipeline inspection and underwater archaeology [1–3]. Generally speaking, in an underwater environment, the contrast of the acquired image is very low, so it is difficult to effectively process and analyze the image information. On the one hand, the absorption and scattering of light by the water body make the light containing the object information not ideally imaged, resulting in blurry imaging of underwater objects; on the other hand, the noise formed by stray light will superimpose on the reflected light of the object, resulting in reduced image contrast [4]. Therefore, effective restoration of underwater images and improvement of image clarity have become hot and important issues to be solved urgently [5–7].

At present, the methods to achieve underwater image restoration and improve image clarity mainly include image processing restoration technology and optical restoration technology [7–10]. Among them, existing digital image processing-based restoration technologies predominantly achieves scene detail restoration by processing a single image [10–15]. Image enhancement and reconstruction technologies are two examples of such approaches. The purpose of image enhancement technology is to improve the contrast of objects, without con-

* Corresponding author at: Changchun Institute of Optics, Fine Mechanics and Physics, Chinese Academy of Sciences, Changchun 130033, China.
E-mail address: yaokainan001@126.com (K. Yao).
Peer review under responsibility of Faculty of Engineering, Alexandria University.

https://doi.org/10.1016/j.aej.2021.06.007

sidering the reasons for image degradation. The technology is often simple algorithm, fast processing speed, obvious effect, so the scope of application is wide. However, the technology is greatly affected by the shooting conditions and environment, and the image restoration ability is normal. Histogram equalization technology [8], Retinex technology [9,11], and wavelet transform technology [16] are examples of popular image enhancement technologies. Image restoration technology is based on the physical degradation model, which uses prior knowledge and expectations to estimate the interference factors that impact image clarity, through the inversion of the degradation process, eliminate the influence of interference factors and improve the image clarity. In general, compared with image enhancement technology, image restoration technology will obtain more natural dehazing images. However, the algorithm of this technology is complex, and dehazing the image takes a long time, rendering it unsuitable for real-time processing, in the case of dense turbid medium with heavy scattering, the recovery effect is reduced. Typical restoration techniques include DCP technique [13,14], multi-channel fusion technique [15,17], etc.

Different from image processing dehazed technology, image restoration technology based on optical means focuses more on the acquisition and processing of optical imaging systems and optical information. Such typical methods include multispectral fusion restoration [18], polarization optical imaging restoration [19–27], etc. Among them, the restoration technology based on polarization imaging is one of the most effective optical restoration methods, which can effectively suppress backscattered light to improve image clarity. As the detection distance increases, the intensity of the scene light attenuates and its polarization information almost disappears, while the intensity of backscattered light increases and has obvious polarization characteristics [19]. Polarization restoration technology collects different polarization images of the same scene, performs differential processing or accurately estimates the backscattered light polarization properties, and then deduce the intensity and transmission coefficient of scattered light, and finally achieve the purpose of suppressing scattered light and improving image clarity [19,20]. Moreover, since the scattered light produced by scattering media, such as haze and sand dust, often has partial polarization characteristics, the polarization restoration technology is ideal for various scattering media conditions with a wide variety of applications [22,23]. Especially in the high concentration of scattering media, it has advantages [20]. However, to achieve the purpose of dehazing, two [28] or more [20,29,30] images with different polarization directions are usually needed to estimate the polarization degree of the image, environmental light intensity, and transmittance distribution, and the final restoration result usually requires different parameters to modify them [20,31]. There are many polarization imaging technologies and systems that can meet the above requirements [20,32,33]. The Division-of-Time method [34] is easy to apply and can achieve a high spatial resolution, but the time resolution is always poor, rendering it inefficient for fast-moving objects. The Division-of-Amplitude method [35] and the Division-of-Aperture method [36] will also produce multiple polarization images at the same time, but the system is relatively complex and requires accurate image registration and calibration. The pixel-level polarization camera of the Division-of-Focal-Plane method [37,38] sacrifices spatial resolution and is very expensive.

We suggest a new dehazing approach that incorporates optics and image processing technologies to solve this problem. Firstly, the linear polarization light is used to actively illuminate the underwater object, and then a linear polarizer perpendicular to the polarization direction of the illumination source is placed in front of the camera, so that a large part of the backscattering light and a part of the object light of the object with strong polarization maintaining can be removed by optical means. Finally, inspired by He et al [13], we use the average filtering to quickly solve the transmittance, thus derive the final dehazing image. The results show that in a scattering environment of differing concentrations, the algorithm can produce a high-quality dehazing effect for artifacts made of diverse materials, as well as for gray and color images.

2. Theory

2.1. Image degradation model

Similar to the atmospheric dehazing imaging model, in an underwater environment, the incident light that the sensor receives is split into two parts [19,39]. The intensity information of the target object is found in the reflected light of the target object, which is also known as direct light. Backscatter is the key element in the creation of a haze environment, and it is caused by light scattered by reflecting particles in the water into the detector. Therefore, the obtained light intensity I can be expressed as:

$$I(x) = I_A(x) + I_B(x) \tag{1}$$

where I_A and I_B represent direct light and backscatter, respectively. The object light (represented by J) is what we finally need to retrieve, and its degraded version at the distance of x is denoted as I_A. I_B increases with distance, and when the distance is infinite, I_B is represented by A at this time. Therefore, Equation (1) can be written as [40,41]:

$$I(x) = J(x)t(x) + A(1 - t(x)) \tag{2}$$

where $t(x)$ usually called as the transmittance. From Equations (2), $J(x)$ can be derived as:

$$J(x) = \frac{I(x) - A}{t(x)} + A \tag{3}$$

When obtain A and $t(x)$, the clear images after dehazing can be reconstructed.

2.2. The principle of polarization removal backscatter

The Stokes vector can be used to explain the polarization state and the intensity of radiation, which defined as:

$$S = \begin{pmatrix} I \\ Q \\ U \\ V \end{pmatrix} \tag{4}$$

where the radiation intensity is expressed as I and the Q, U, V components denote the polarization state of the radiation, the following equations can be used to express it:

$$\begin{aligned} I &= E_l^2 + E_r^2 \\ Q &= E_l^2 - E_r^2 \\ U &= 2E_lE_r\cos\delta \\ V &= 2E_lE_r\sin\delta \end{aligned} \tag{5}$$

The E_r and E_l represent the electric field components of the scattered wave perpendicular and parallel to the reference plane, respectively, and δ represents the relative phase.

The 4 × 4 Mueller matrix represents the depolarization effect of the target or medium on the incident light.

The scattered light and incident radiation typically have separate polarization states, and the change process can be expressed as the matrix multiplication of M.

$$S_o = MS_i \Rightarrow \begin{pmatrix} I_o \\ Q_o \\ U_o \\ V_o \end{pmatrix} = \begin{pmatrix} M_{11} & M_{12} & M_{13} & M_{14} \\ M_{21} & M_{22} & M_{23} & M_{24} \\ M_{31} & M_{32} & M_{33} & M_{34} \\ M_{41} & M_{42} & M_{43} & M_{44} \end{pmatrix} \begin{pmatrix} I_i \\ Q_i \\ U_i \\ V_i \end{pmatrix} \tag{6}$$

$$M = \begin{pmatrix} M_{11} & M_{12} & M_{13} & M_{14} \\ M_{21} & M_{22} & M_{23} & M_{24} \\ M_{31} & M_{32} & M_{33} & M_{34} \\ M_{41} & M_{42} & M_{43} & M_{44} \end{pmatrix} \tag{7}$$

where I_i, Q_i, U_i, V_i are the Stokes vector components of incident radiation, respectively. Where I_o, Q_o, U_o, V_o are the Stokes vector components of scattered light, respectively.

When the wavelength of the radiation exceeds the diameter of the scattering particles, Rayleigh scattering occurs. In this case, the normalized Mueller matrix of the medium is as follows [42,43]:

$$M(\theta) = \begin{bmatrix} 1 & b(\theta) & 0 & 0 \\ b(\theta) & 1 & 0 & 0 \\ 0 & 0 & d(\theta) & 0 \\ 0 & 0 & 0 & d(\theta) \end{bmatrix} \tag{8}$$

where:

$$b(\theta) = \frac{-1 + \cos^2\theta}{1 + \cos^2\theta}, \quad d(\theta) = \frac{2\cos\theta}{1 + \cos^2\theta} \tag{9}$$

and θ is the scattering angle.

Therefore, under the condition of backscattering with the scattering angle is 180 degrees, the Mueller matrix of Rayleigh scattering assumes as follows:

$$M = \begin{pmatrix} 1 & 0 & 0 & 0 \\ 0 & 1 & 0 & 0 \\ 0 & 0 & -1 & 0 \\ 0 & 0 & 0 & -1 \end{pmatrix} \tag{10}$$

Therefore, with the aid of Stokes-Mueller formalism, it can be deduced that under Rayleigh scattering conditions, backscattering with a reflection angle of 180 degrees preserves the vertical or horizontal linear polarization of the incident light.

2.3. Fast dehazing method based on average filtering to estimate the backscatter light

Through the method in Section 2.2, partial backscattering can be removed by polarization, but complete dehazing cannot be achieved. In order to be able to remove the remaining part of haze, we use the method of quickly estimating atmospheric veil based on average filtering to achieve rapid dehazing. The proposed dehazing algorithm will be described in detail. According to Equations (3), the key to dehazing is to calculate the transmission and evaluate the global atmospheric light.

He et al. [13] discovered that any pixels in at least one color channel in most non-sky patches of haze-free images are still very low in intensity. As a consequence, the DCP dehazing approach is advised. The dark channel of the image is defined as follows:

$$J^{dark}(x) = \min_{y\in\Omega(x)}\left(\min_{c\in\Omega\{r,g,b\}} J^c(y)\right) \tag{11}$$

where $\Omega(x)$ represents a local patch centered at x and J^c represents the color channel of J. This specific area of the dark channel will tend to zero. Equations (2) and (11) are combined to give the following expression for the transmittance t:

$$t(x) = 1 - w\min_{y\in\Omega(x)}\left(\min_{c\in\Omega\{r,g,b\}} \frac{I^c(y)}{A^c}\right) \tag{12}$$

where A^c is the atmospheric light of the image with pixel intensity value between [0,1] in each color channel. The inclusion of constant w ($0 < w < 1$) retains some haze, taking the dehazing image closer to reality, which makes the dehazing image closer to the real scene. The measured atmospheric light and transmittance map can be used to restore the scene radiance using the following methods.

$$J(x) = \frac{I(x) - A}{\max(t(x), t_0)} + A \tag{13}$$

where t_0 is the minimum boundary of t, and its value usually set to 0.1. This is to avoid too much noise in J when t is close to 0. Using the transmission image obtained by Equation (12) to recover the scene radiance may result in undesirable dehazing artifacts, such as halo or block artifacts. The reason for this phenomenon is that the transmittance in the selected color block Ω is not a constant. In order to mitigate this effect, some scholars proposed a soft matting technique to refine the transmission map, which solved this problem nicely.

As we mentioned before, the disadvantage of this method is time complexity and high computational cost. For real-time applications of image haze removal, time cost is a key issue that needs to be resolved. To improve the performance of this method, we can quantify the transmission map using the average filtering technique.

In Equations (1) the backscattered light can be express as:

$$I_B(x) = A(1 - t(x)) \tag{14}$$

As a result, $t(x)$ can be estimated by I_B as:

$$\tilde{t}(x) = 1 - \frac{I_B(x)}{A} \tag{15}$$

To approximate the backscattered light $I_B(x)$, we use the image blur algorithm for $I(x)$. Image blur can be achieved by image filtering. For the source image $f(x\ ,y)$ and the weighting kernel $w(i,j)$, the result image $g(x,y)$ is their convolution, which can be written as:

$$g(x,y) = \sum_{i=-r}^{r}\sum_{j=-r}^{r} f(x+\mathrm{i}, y+j) * w(i,j) \tag{16}$$

where r is radius of kernel, an odd number is selected generally. To meet the demands of real-time applications while also increasing execution speed, we reduce the complexity of the algorithm as much as possible, so we use the average filter.

We assume that the width and height of the image is *width* and *height* respectively, and the radius of convolution kernel is *radius*. Then the time complexity of convolution is O (*width* * *height* * 2 * (2 * *radius* + 1)^2).

In order to speed up the algorithm, the convolution kernel is divided into two convolution kernels in a one-dimensional horizontal direction and a one-dimensional vertical direction. The entire convolution process is regarded as a one-dimensional sliding window average filter on the row and column, so the complexity of convolution is reduced to O (*width* * *height* * (2 * *radius* + 1) * 2). In the sliding process of the one-dimensional window, a large number of elements in adjacent windows overlap. The entire sliding process can be seen as a process of continuously entering and leaving the "queue". Every time the window moves one pixel to the right, it is equivalent to the leftmost pixel leaving the queue and the rightmost pixel entering the queue. The filtering result of the current pixel is the sum of the elements in the current queue and then averaged, while the elements that have been in the queue before and after do not need to be added repeatedly, and the speed is increased by avoiding repeated calculations. In this way, we get an algorithm that is independent of the filter size, and its complexity is O(*width* * *height*).

For the source image $I(x)$, the filtered image $I_f(x)$ can be obtained through the fast average filtering, which can be simplified as:

$$I_f(x) = average_{sv}(I(x)) \tag{17}$$

where sv is the radius of the average filter. We approximate the backscatter light as:

$$I_B(x) = I_f(x) - \sigma_{I_f} \tag{18}$$

where σ_{I_f} is the standard deviation of I_f .

In the previous researches, there are many methods to estimate background light A. Tan [41], for example, assumes the global atmospheric light A to be the brightest pixel value in the scene radiation. He [13] takes the brightest 0.1% pixel in the dark channel as the maximum haze area, and selects the maximum value in the corresponding area in the original image as the atmospheric light A. The average value of the brightest 0.1 percent pixels in the original image is calculated as atmospheric light A in this paper. We can substitute background light A and I_B into Equations (15) and Equations (3) to get the dehazing image J.

3. Experiments and discussion

To validate the image recovery method mentioned in Section 2.3, we conduct an underwater imaging experiment.

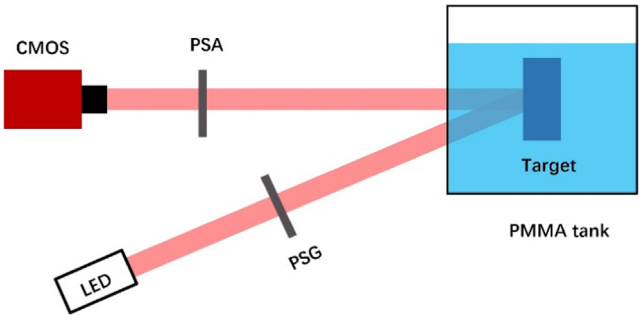

Fig. 1 Schematic of the experimental setup for underwater imaging.

Fig. 1 illustrates the experimental setup. A light source made of white LEDs illuminates the target. The imaging system is a 12-bit digital CMOS sensor (MC023CG-SY-FL) with 1936 × 1216 pixels. A polarizer is placed in front of the light source and CMOS respectively. We filled a transparent container (400 mm × 200 mm × 400 mm) with water and mixed clear water with skim milk to make the water turbid.

In the experimental device, the LED light source passes through the linear polarizer PSG to become linearly polarized light, then reaches the surface of the object through the water body, then passes through the linear polarizer PSA after reflection, finally enters the CMOS. In the experiment, a mixed solution of skimmed milk and tap water was used to simulate the impact of the underwater environment on the imaging results, the skimmed milk mainly contains biological protein particles (particle size is about 0.04–0.3um). The mixed solution can well simulate the Rayleigh scattering of light waves during the propagation of seawater. The results of this experiment were collected in two solutions with different concentrations. The first concentration consisted of 15L tap water and 15 ml milk, while the second consisted of 15L tap water and 20 ml milk. The experiment is divided into 3 cases: (1) the image is obtained when the linear polarizer PSA is not added; (2) the polarization direction of the polarizer PSA is adjusted to be parallel to the polarization direction of the polarizer PSG to obtain the image; (3) the polarization direction of the polarizer PSA is adjusted to be cross-perpendicular to the polarization direction of the polarizer PSG to obtain the image.

3.1. Polarization removes part of the backscattered light

We use a plastic plate with the letter K as the observation target. The surface of the target is relatively rough and has strong depolarization. As polarized light hits a target, the reflected light loses its polarization. The images obtained in the experiment are as follows.

As we can see from Fig. 2 that in the three images on the top row, the targets in (a) and (b) are relatively blurred, and the visibility of the targets in (c) has been greatly improved; In the three images in the bottom row, the target in (d) and (e) is almost invisible, and the target can be seen in (f). The findings of the experiments demonstrate that the polarizer cross-perpendicular to the polarizer parallel and without the polarizer can obtain better imaging results, because the polarizer can filter out part of the backscatter when the polarizer is cross-perpendicular. At the same time, the results derived in

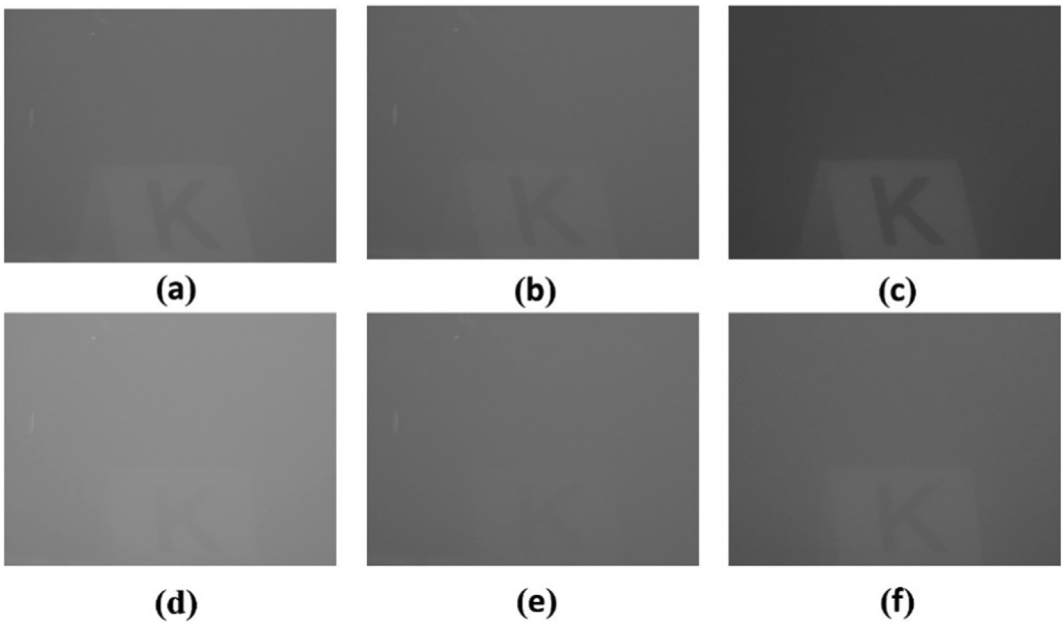

Fig. 2 Target images acquired in a turbid solution, where the top row is the image acquired in a low turbidity conditions, and the bottom row is the image acquired in a high turbidity condition. (a) and (d) are the images obtained directly without the polarizer; (b) and (e) are the images obtained in the parallel state of the polarizer; (c) and (f) are the images obtained in the cross-perpendicular state of the polarizer.

Section 2.2 are also verified: in Rayleigh scattering, the backscattering of linearly polarized light maintains the original polarization direction.

In the next, we use the value of measure of enhancement (EME) to calculate the image quality [44], and define the EME as

$$EME = \left| \frac{1}{k_1 k_2} \sum_{l=1}^{k_2} \sum_{k=1}^{k_1} 20\log \frac{i^{\omega}_{\max;k,l}(x,y)}{i^{\omega}_{\min;k,l}(x,y) + q} \right| \tag{19}$$

The underwater image is equally divided into k1 × k2 small blocks according to the pixel distribution, (k,l) represents the position sequence where each small block is located, $i^{\omega}_{\max;k,l}(x,y)$ and $i^{\omega}_{\min;k,l}(x,y)$ represent the maximum pixel value and minimum pixel value in the (k,l) small block ω in the image sequence. q is an extremely small constant to avoid the denominator being 0. The higher the EME value, the higher the image quality. As can be seen in Table 1, cross-perpendicular polarization images produce greater contrast.

Table 1 The EME value of the images in Fig. 2.

Fig. 2(a)	Fig. 2(b)	Fig. 2(c)
EME 0.8440	1.0831	1.9527
Fig. 2(d)	Fig. 2(e)	Fig. 2(f)
EME 0.5406	0.8369	1.5101

3.2. Our method dehazes gray-scale polarization images

Because only part of the backscattering can be removed through Section 3.1, the algorithm described in Section 2.3 is applied to the obtained polarization image to improve its clarity even more. The target is a ceramic water cup, and the following are the outcomes of the algorithm processing.

As seen in Fig. 3, the clarity of (c) is greater than (a), (b) and the clarity of (f) is higher than (d), (e). It shows that the backscatter that cannot be removed by polarization can be removed by our algorithm. Our algorithm has a good effect on the dehazing of gray-scale polarization images.

For the purpose of comparing the execution efficiency of the algorithm, our method, DCP and Fast DCP (He has proposed a new method called Guided Image Filtering [45] to replace the Soft Matting), the three algorithms are all implemented in matlab code, process 4 resolution images on a computer with an Intel Core i7 and clocked at 2.20 GHz. In order to eliminate the contingency factor, the time consumption of the algorithm is obtained by averaging the time of processing 10 images of the same resolution. The final average time consumption is as follows.

It can be seen from Table 2 that although the speed of fast DCP has increased a lot compared to DCP, it still cannot meet the needs of real-time applications. Our method significantly reduces the processing time, and the time consumption is only about 2 percent of fast DCP for experimental images. For 1 k resolution images, real-time requirements can be fully met, and if the algorithm is changed to a more efficient C code, then higher resolution images can be processed in real time.

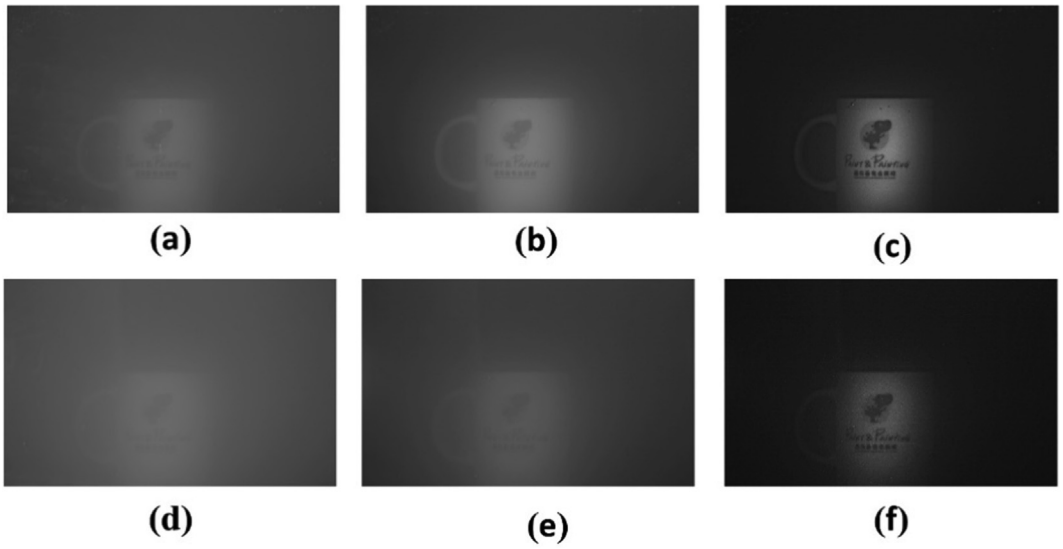

Fig. 3 The acquired grayscale water cup image, where the top row is the image acquired under low turbidity conditions, and the bottom row is the image acquired under high turbidity conditions. (a) and (d) are the images obtained directly without the polarizer;(b) and (e) are the images obtained in the cross-perpendicular state of the polarizer;(c) and (f) are the images obtained in the cross-perpendicular state of the polarizer and then restored by our dehazing method.

Table 2 Time-consuming comparison of three methods.

Image size	608 × 968	1216 × 1936	1824 × 2904	2432 × 3872
DCP(s)	7.334	31.506	76.659	156.394
fast DCP(s)	2.506	8.518	20.230	35.117
our method(s)	0.041	0.173	0.387	0.702

3.3. Our method dehazes color-scale polarization images

We then test the dehazing effect of the color image to verify the versatility of the algorithm. Here, we do not consider the absorption of light waves by water bodies, and it is approximately considered that the backscattered light of the three channels of the color image is equal. There are three stages in the estimation process: first, the color image is converted to a grayscale image, and then the grayscale image is calculated using Equations (17) and (18) to obtain I_B, finally, each channel of the color image uses I_B to solve the dehazing results separately. The school badge is used as the goal, and the following are the results of the algorithm processing.

The color image has the same dehazing effects as the grayscale image, as seen in Fig. 4, and the combination of the polarization and our algorithm can achieve the best dehazing effect. Since the small protein particles in the solution mainly scatter visible light with shorter wavelengths, it can be seen in (a), (b), (d), and (e) that the solution is slightly blue, while (c), (f) after dehazing can also be seen to be blue, so dehazing the color image using our algorithm will not change the color of the original image.

4. Conclusions

The most representative image processing dehazing technology based on the physical degradation model is the DCP, which can obtain a more natural dehazing image. However, the algorithm is more complicated, the dehazing processing is time-consuming, not suitable for real-time processing, and the recovery effect is limited under strong scattering media. The image dehazing technology based on polarization imaging usually needs two or more images of the same scene with different polarization directions to estimate the polarization characteristics of backscattered light, and in order to obtain better dehazing images, the bias parameter is usually required to resolve issues relating to the quantum noise of sensor. However, the bias parameter is different in different scattering environments or three different channels of the RGB image, which reduces the robustness of this method, and acquiring multiple images will either sacrifice time resolution or spatial resolution. We propose an optimization algorithm in this paper. First, use a linear polarizer to filter out a part of the backscattering of the strong scattering medium through an optical method, and then use the average filter technology to estimate the

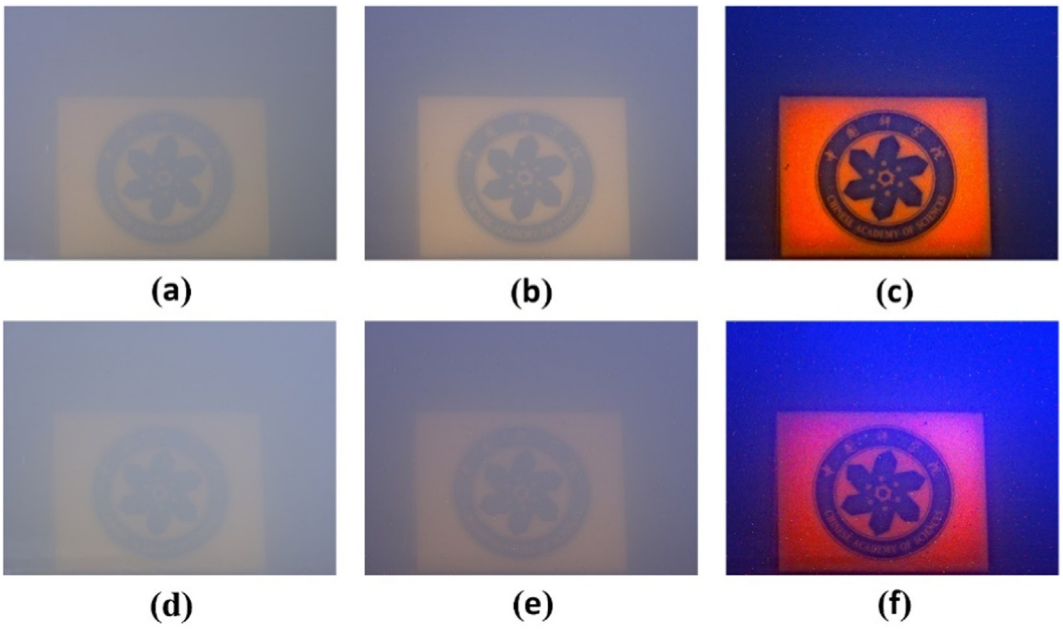

Fig. 4 The acquired color school badge image, where the top row is the image acquired under low turbidity conditions, and the bottom row is the image acquired under high turbidity conditions. (a) and (d) are the images obtained directly without the polarizer; (b) and (e) are the images obtained in the cross-perpendicular state of the polarizer; (c) and (f) are the images obtained in the cross-perpendicular state of the polarizer and then restored by our dehazing method.

remaining part of the backscattered light to quickly restore the image. Our dehazing method not only overcomes the limitation of its limited recovery effect under strong scattering media, but also the time-consuming is only 2 percent of fast DCP method when processing 1 k resolution images and meets real-time requirements. The procedure is effective and robust under various imaging conditions, according to the findings of the experiments.

Declaration of Competing Interest

The authors declare that they have no known competing financial interests or personal relationships that could have appeared to influence the work reported in this paper.

References

[1] A. Ortiz, M. Simó, G. Oliver, A vision system for an underwater cable tracker, Mach. Vis. Appl. 13 (2002) 129–140.
[2] D.F. Coleman, J.B. Newman, R.D. Ballard, Design and implementation of advanced underwater imaging systems for deep sea marine archaeological surveys, in: OCEANS 2000 MTS/IEEE Conference and Exhibition. Conference Proceedings (Cat. No. 00CH37158). IEEE, 2000, pp. 661–665.
[3] P.J.A. Alphonse, K.V. Sriharsha, Depth perception in a single RGB camera using body dimensions and centroid property, Traitement du Signal 37 (2020) 333–340.
[4] J.S. Jaffe, Computer modeling and the design of optimal underwater imaging systems, IEEE J. Oceanic Eng. 15 (1990) 101–111.
[5] J.S. Jaffe, K.D. Moore, J. McLean, M.P. Strand, Underwater optical imaging: status and prospects, Oceanography 14 (2001) 66–76.
[6] H. Singh, J. Adams, D. Mindell, B. Foley, Imaging underwater for archaeology, Journal of Field Archaeology 27 (2000) 319–328.
[7] Y. Xu, J. Wen, L. Fei, Z. Zhang, Review of video and image defogging algorithms and related studies on image restoration and enhancement, IEEE Access 4 (2015) 165–188.
[8] J. Liu, X. Wang, M. Chen, S. Liu, X. Zhou, Z. Shao, P. Liu, Thin cloud removal from single satellite images, Opt. Express 22 (2014) 618–632.
[9] G.S. Rajput, Z.U. Rahman, Hazard detection on runways using image processing techniques, in: Enhanced and Synthetic Vision 2008, International Society for Optics and Photonics, 2008, p. 69570D.
[10] S. Emberton, L. Chittka, A. Cavallaro, Underwater image and video dehazing with pure haze region segmentation, Comput. Vis. Image Underst. 168 (2018) 145–156.
[11] S. Serikawa, H. Lu, Underwater image dehazing using joint trilateral filter, Comput. Electr. Eng. 40 (2014) 41–50.
[12] M. Jayasree, G. Thavaseelan, Underwater color image enhancement using wavelength compensation and dehazing, International Journal of Computer Science and Engineering Communications 2 (2014) 389–393.
[13] K. He, J. Sun, X. Tang, Single image haze removal using dark channel prior, IEEE Trans. Pattern Anal. Mach. Intell. 33 (2010) 2341–2353.
[14] R. Sathya, M. Bharathi, G. Dhivyasri, in: Underwater image enhancement by dark channel prior, in, 2015, pp. 1119–1123.
[15] H. Lu, Y. Li, S. Nakashima, H. Kim, S. Serikawa, Underwater image super-resolution by descattering and fusion, IEEE Access 5 (2017) 670–679.
[16] F. Russo, An image enhancement technique combining sharpening and noise reduction, IEEE Trans. Instrum. Meas. 51 (2002) 824–828.
[17] W. Zhang, J. Liang, L. Ren, H. Ju, E. Qu, Z. Bai, Y. Tang, Z. Wu, Real-time image haze removal using an aperture-division polarimetric camera, Appl. Opt. 56 (2017) 942–947.
[18] J. Liang, W. Zhang, L. Ren, H. Ju, E. Qu, Polarimetric dehazing method for visibility improvement based on visible and infrared image fusion, Appl. Opt. 55 (2016) 8221–8226.

[19] Y.Y. Schechner, N. Karpel, Recovery of underwater visibility and structure by polarization analysis, IEEE J. Oceanic Eng. 30 (2005) 570–587.
[20] J. Liang, L. Ren, H. Ju, W. Zhang, E. Qu, Polarimetric dehazing method for dense haze removal based on distribution analysis of angle of polarization, Opt. Express 23 (2015) 26146–26157.
[21] B. Huang, T. Liu, H. Hu, J. Han, M. Yu, Underwater image recovery considering polarization effects of objects, Opt. Express 24 (2016) 9826–9838.
[22] J. Cariou, B. Le Jeune, J. Lotrian, Y. Guern, Polarization effects of seawater and underwater targets, Appl. Opt. 29 (1990) 1689–1695.
[23] Y.Y. Schechner, N. Karpel, Clear underwater vision, in: Proceedings of the 2004 IEEE Computer Society Conference on Computer Vision and Pattern Recognition, 2004. CVPR 2004. IEEE, 2004, pp. I–I.
[24] J. Mudge, M. Virgen, Real time polarimetric dehazing, Appl. Opt. 52 (2013) 1932–1938.
[25] W. Zhang, J. Liang, H. Ju, L. Ren, E. Qu, Z. Wu, A robust haze-removal scheme in polarimetric dehazing imaging based on automatic identification of sky region, Opt. Laser Technol. 86 (2016) 145–151.
[26] Y. Qu, Z. Zou, Non-sky polarization-based dehazing algorithm for non-specular objects using polarization difference and global scene feature, Opt. Express 25 (2017) 25004–25022.
[27] J.S. Tyo, M. Rowe, E. Pugh, N. Engheta, Target detection in optically scattering media by polarization-difference imaging, Appl. Opt. 35 (1996) 1855–1870.
[28] Y.Y. Schechner, S.G. Narasimhan, S.K. Nayar, Instant dehazing of images using polarization, in, in: Proceedings of the 2001 IEEE Computer Society Conference on Computer Vision and Pattern Recognition. CVPR 2001, 2001, p. pp. I-I..
[29] J. Liang, H. Ju, L. Ren, L. Yang, R. Liang, Generalized polarimetric dehazing method based on low-pass filtering in frequency domain, Sensors 20 (2020) 1729.
[30] L. Yang, J. Liang, W. Zhang, H. Ju, L. Ren, X. Shao, Underwater polarimetric imaging for visibility enhancement utilizing active unpolarized illumination, Opt. Commun. 438 (2019) 96–101.
[31] J. Liang, L. Ren, E. Qu, B. Hu, Y. Wang, Method for enhancing visibility of hazy images based on polarimetric imaging, Photonics Res. 2 (2014) 38–44.
[32] F. Parnet, J. Fade, N. Ortega-Quijano, L. Frein, M. Alouini, Free-space active polarimetric imager operating at 1.55 mm by orthogonality breaking sensing, Opt. Lett. 42 (2017) 723–726.
[33] J. Chu, Z. Wang, L. Guan, Z. Liu, Y. Wang, R. Zhang, Integrated polarization dependent photodetector and its application for polarization navigation, IEEE Photonics Technol. Lett. 26 (2014) 469–472.
[34] J.S. Tyo, D.L. Goldstein, D.B. Chenault, J.A. Shaw, Review of passive imaging polarimetry for remote sensing applications, Appl. Opt. 45 (2006) 5453–5469.
[35] J. Mudge, M. Virgen, Near-infrared simultaneous Stokes imaging polarimeter: integration, field acquisitions, and instrument error estimation, in: Polarization Science and Remote Sensing V. International Society for Optics and Photonics, 2011, p. 81600B.
[36] H. Ju, L. Ren, J. Liang, E. Qu, Z. Bai, Method for Mueller matrix acquisition based on a division-of-aperture simultaneous polarimetric imaging technique, J. Quant. Spectrosc. Radiat. Transfer 225 (2019) 39–44.
[37] Z. Zhang, F. Dong, T. Cheng, K. Qiu, Q. Zhang, W. Chu, X. Wu, Nano-fabricated pixelated micropolarizer array for visible imaging polarimetry, Rev. Sci. Instrum. 85 (2014) 105002.
[38] K. Shinoda, Y. Ohtera, M. Hasegawa, Snapshot multispectral polarization imaging using a photonic crystal filter array, Opt. Express 26 (2018) 15948–15961.
[39] Y.Y. Schechner, S.G. Narasimhan, S.K. Nayar, Polarization-based vision through haze, Appl. Opt. 42 (2003) 511–525.
[40] R. Fattal, Single image dehazing, ACM Transactions on Graphics (TOG) 27 (2008) 1–9.
[41] R.T. Tan, Visibility in bad weather from a single image, in: 2008 IEEE Conference on Computer Vision and Pattern Recognition. IEEE, 2008, pp. 1–8.
[42] L. Bartolini, L. De Dominicis, M.F. De Collibus, G. Fornetti, M. Francucci, M. Guarneri, E. Paglia, C. Poggi, R. Ricci, Polarimetry as tool to improve phase measurement in an amplitude modulated laser for submarine archaeological sites inspection, in: O3A: Optics for Arts, Architecture, and Archaeology, International Society for Optics and Photonics, 2007, p. 66180I.
[43] G.W. Kattawar, M.J. Rakovĭc, Virtues of Mueller matrix imaging for underwater target detection. Applied Optics 38 (1999) 6431–6438.
[44] S.S. Agaian, K. Panetta, A.M. Grigoryan, Transform-based image enhancement algorithms with performance measure, IEEE Trans. Image Process. 10 (2001) 367–382.
[45] K. He, J. Sun, X. Tang, Guided image filtering, IEEE Trans. Pattern Anal. Mach. Intell. 35 (2012) 1397–1409.